This article has been accepted for inclusion in a future issue of this journal. Content is final as presented, with the exception of pagination.

Analysis, Comparison, and Experimental Validation of a Class AB Voltage Follower With Enhanced Bandwidth and Slew Rate

Anindita Paul, *Member, IEEE*, Jaime Ramírez-Angulo, *Fellow, IEEE*, and Antonio Torralba, *Senior Member, IEEE*

***Abstract*— This paper describes a bandwidth (BW)- and slew rate (SR)-enhanced class AB voltage follower (VF). A thorough small signal analysis of the proposed and a state-of-the-art AB-enhanced VF is presented to compare their performance. The proposed circuit has 50-MHz BW, 19.5-V/μs SR, and a BW figure of merit of 41.6 (MHz × pF/μW) for C_L = 50 pF. It provides 13 times higher current efficiency and 15 times higher BW than the conventional VF with equal 60-μW static power dissipation. The experimental and simulation results of a fabricated test chip in the 130-nm CMOS technology validate the proposed circuit.**

***Index Terms*— Analog integrated circuits, CMOS technology, MOSFET circuits, negative feedback, voltage follower (VF), wide bandwidth (BW).**

I. Introduction

The bandwidth (BW) of the CMOS conventional voltage follower (CNV-VF), shown in Fig. 1, is given approximately by $\mathrm{BW_{CNV}} = g_{m1}/2\pi C_L$, where g_{m1} is the transconductance of M_1 and C_L is the load capacitance. The negative slew rate (SR^-) of the circuit is limited by the bias current I_B to a value $\mathrm{SR}^- = I_B/C_L$, while the positive slew rate (SR^+) can have a relatively large value, since the maximum positive output current is not limited by I_B. In practice, a symmetrical slew rate (SR) is desirable, since the lowest of the positive and negative SRs limits the large signal speed. This means that in practice, the SR corresponds to min $\{\mathrm{SR}^+, \mathrm{SR}^-\}$. Both the SR and the BW can be increased at the expense of increasing I_B and consequently the static power dissipation. In the modern submicrometer CMOS technology, low power consumption is a key requirement for increasing the battery life of portable systems [1]–[3]. Class AB VFs (CNV-AB-VFs) can boost the maximum negative output current (and consequently SR^-) without increasing the static power dissipation essentially. Till date, many different CNV-AB-VFs have been reported that have improved the SR without improving the BW. Often, the desired class AB operation is achieved at the expense of increasing the supply voltage, the power dissipation, circuit complexity, and the silicon area. A comprehensive survey of buffers/VFs can be found in [4]. For high-speed applications, both the SR and the BW are equally important (see discussion in Section V). In this paper, we propose a simple and power efficient CNV-AB-VF. The proposed CNV-AB-VF dissipates the same quiescent power as a CNV-VF but has much higher SR and BW. Three figures of merits can be used to characterize and compare the performance of VFs. First, the current enhancement figure of merit, $\mathrm{FOM_{CE}} = I_{\mathrm{outMAX}}/I_{Q\mathrm{total}}$ [5]–[7], where I_{outMAX} is the maximum output current and $I_{Q\mathrm{total}}$ is the total quiescent current. This is related to the SR improvement and the large signal performance of the circuit. Second, the BW figure of merit [6]–[8], $\mathrm{FOM_{BW}} = \mathrm{BW(MHz)}C_L(\mathrm{pF})/P^Q(\mu\mathrm{W})$, where P^Q is the total quiescent power dissipation of the circuit. Since $\mathrm{FOM_{CE}}$ determines the speed limitation for large signals and $\mathrm{FOM_{BW}}$ limits the speed of small signals, a third global speed figure of merit [6], [7] can also be defined that corresponds to the geometric mean of the previous two figures of merit $\mathrm{FOM_{GLB}} = (\mathrm{FOM_{CE}FOM_{BW}})^{1/2}$.

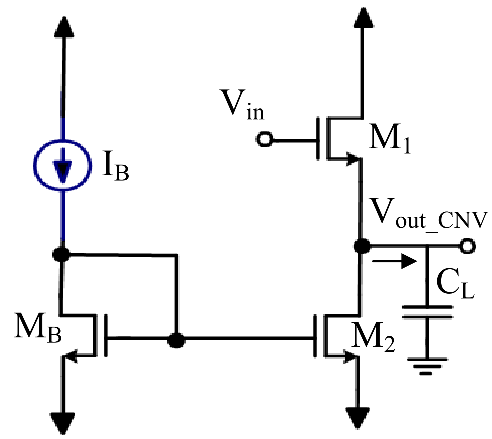

Fig. 1. CNV-VF.

Manuscript received October 15, 2018; revised January 25, 2019; accepted February 26, 2019. This work was supported by the Spanish Ministry of Economy and Competitiveness under Project TEC2015-71072-C3-3-R. *(Corresponding author: Anindita Paul.)*

A. Paul is with the Klipsch School of Electrical and Computer Engineering, New Mexico State University, Las Cruces, NM 88003 USA (e-mail: apaul03@nmsu.edu).

J. Ramírez-Angulo is with the Klipsch School of Electrical and Computer Engineering, New Mexico State University, Las Cruces, NM 88003 USA, and also with the National Institute of Astrophysics, Optics and Electronics (INAOE), Puebla 72000, Mexico (e-mail: jairamir@nmsu.edu).

A. Torralba is with the Departamento de Ingeniería Electrónica, Escuela Superior de Ingeniería, University of Seville, 41092 Seville, Spain (e-mail: torralba@us.es).

Color versions of one or more of the figures in this paper are available online at http://ieeexplore.ieee.org.

Digital Object Identifier 10.1109/TVLSI.2019.2903116

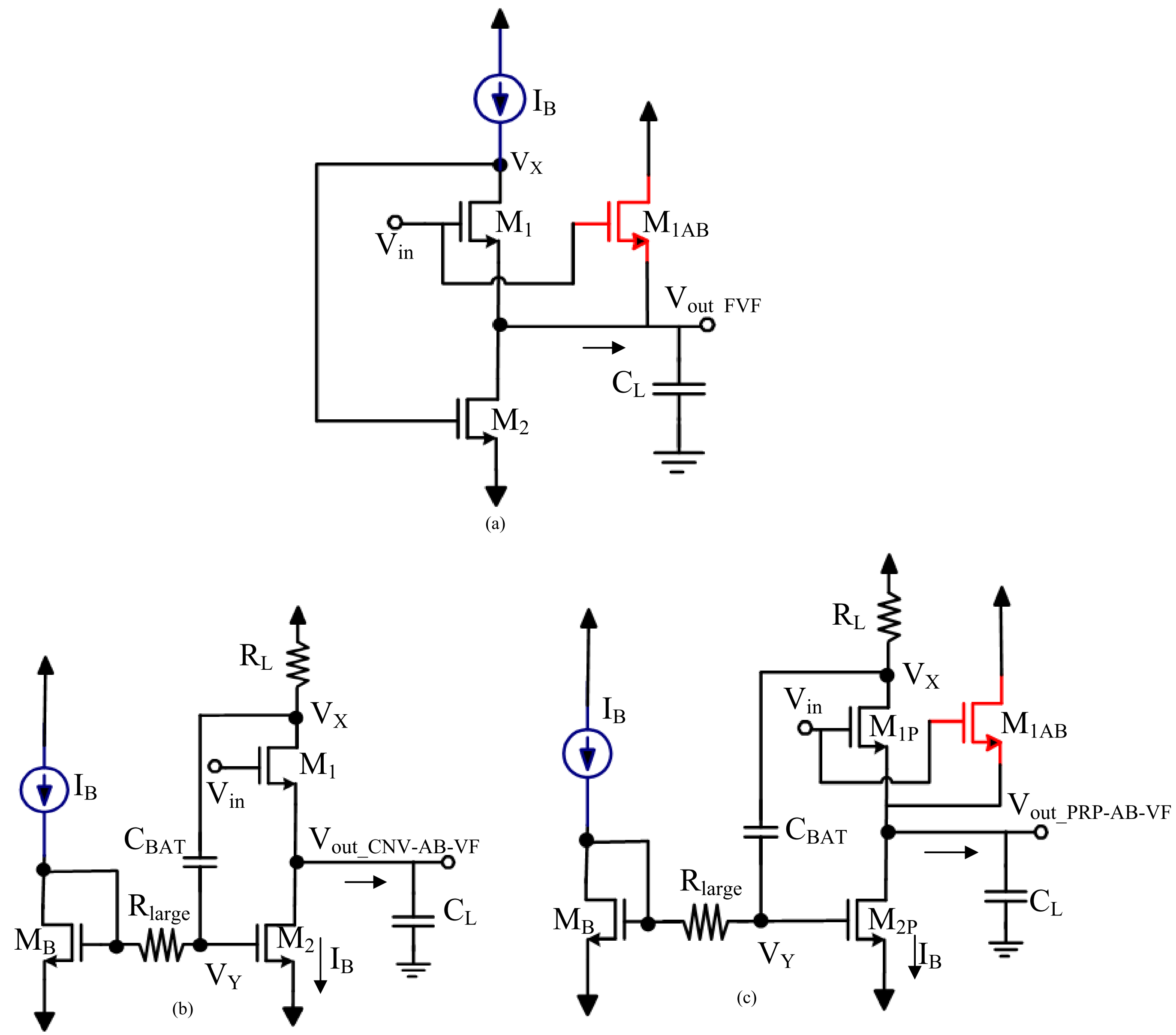

Fig. 2. CMOS CNV-AB-VFs. (a) CMOS FVF reported in [9]. (b) CMOS CNV-AB-VF reported in [10]. (c) Proposed CMOS CNV-AB-VF.

II. Proposed Voltage Follower

Fig. 2(a) shows a class AB flipped VF (FVF) reported in [9] with an additional transistor M_{1AB}, which operates as a CNV-VF and can improve SR^+. However, its output swing is limited by the gate–source voltage of M_2. The input/output peak-to-peak swing is given by $V_{\text{inpp}} = V_T - V_{\text{DSsat}}$, where V_T is the threshold voltage of the transistor. This swing is very small and independent of the supply voltage. This is a very serious limitation, since in the modern technology, lower values of threshold voltage ($V_T \sim 0.4$ V) are used. Maximum peak output signals of the circuit in [9] with a low distortion are on the order of only 0.15 V. Fig. 2(b) shows a CNV-AB-VF (CNV-AB-VF) reported in [10] that has a resistor R_L inserted between the drain of M_1 and V_{DD}. M_1 and M_2 have equal quiescent currents I_B. It can be considered as a dynamic FVF without the swing limitations of the circuit in Fig. 2(a), since the dc operating points at node V_x is independent of the dc operating point at node V_Y and they are connected in the presence of ac signals. The circuit in Fig. 2(b) operates as follows: transient variations in V_{in} generate variations in V_x which are 180° out of phase with V_{in}. These variations are transferred from node V_X to node V_Y using a capacitor C_{BAT} that acts as a floating battery for fast changes in V_X. Furthermore, R_{large} and C_{BAT} form a high-pass circuit for signals passing from V_X to V_Y. This changes the current of M_2 as a function of the variations in V_{in}. Negative (positive) values of V_{in} leads to positive (negative) values in V_X and V_Y, which increase (decrease) the dynamic drain current of M_2. This leads to maximum negative output currents that can be essentially larger than I_B and therefore much higher negative SR than the CNV-VF. An additional advantage of the SR enhancement circuit (R_L, R_{large}, and C_{BAT}) is that the local negative feedback through C_{BAT} in the presence of ac signal decreases the output impedance of the follower by the gain $1 + g_{m2}R_{\text{L}}$ of the negative feedback loop. This also

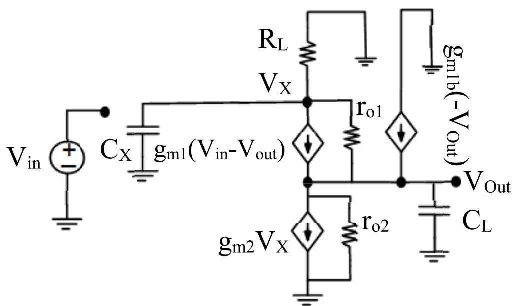

Fig. 3. Small signal analysis of CNV-AB-VF [10].

helps to enhance the BW of the follower, as explained in Section III. In the circuit shown in Fig. 2(b), both the BW and the maximum negative output current (and SR$^-$) increase with R_L. However, the increase of R_L leads to a decrease in the maximum positive output current (and in the SR$^+$), since it is in series with the drain of M_1. This does not allow optimizing SR$^+$, SR$^-$, and BW simultaneously. The proposed VF is shown in Fig. 2(c). It overcomes the limitations of the FVF shown in Fig. 2(a) and of the CNV-AB-VF shown in Fig. 2(b). It is derived by merging the conventional follower in Fig. 1 with the circuit in Fig. 2(b). This is done by adding a transistor M_{1AB} connected as a CNV-VF. M_{1AB} can provide a large positive output current which is independent of the value of R_L. To maintain equal quiescent power dissipation as the CNV-AB-VF and the CNV-VF, the current mirror ratio W_{2P}/W_B of the proposed VF is 1:1 where W_{2P} and W_B are the widths of M_{2P} and M_B. From this point, the proposed circuit in Fig. 2(c) will be denoted as "PRP-AB-VF." As it is shown in Section III, the PRP-AB-VF can deliver simultaneously nearly symmetric and large maximum positive and negative output currents and exhibits moderate-to-high BW enhancement with little area overhead and with the same static power dissipation, as the CNV-VF in Fig. 1. In this paper, the PRP-AB-VF is intended to be used as a buffer for amplifiers. In order to perform a comparison, the small signal analysis of the circuit in [10, Fig. 2(b)] is also included here, since [10] does not include the analysis of the circuit's BW. The focus of this paper is to demonstrate that the proposed circuit has significantly enhanced BW with respect to the circuit shown in Fig. 2(b) and simultaneously high symmetrical SR. The circuit in Fig. 2(a) is not included in the comparison due to the swing limitations.

III. Small Signal Analysis of CNV-AB-VF Circuit Reported in [10]

In this section, a small signal analysis of the CNV-AB-VF circuit in Fig. 2(b) is presented. Transistors M_1 and M_2 have equal dimensions (W/L), the same quiescent current I_B, and the same transconductance gains $g_{m1} = g_{m2} = g_m$. At frequencies higher than $f_0 = 1/(2\pi R_{\text{large}} C_{\text{BAT}})$, the capacitor C_{BAT} acts as a short circuit that connects nodes V_X and V_Y and provides dynamic negative feedback. This negative feedback helps to enhance the BW of the CNV-AB-VF follower, according to the analysis shown in the following.

Fig. 3 shows the ac equivalent circuit of Fig. 2(b) for $f \geq f_0 = 1/(2\pi R_{\text{large}} C_{\text{BAT}})$. The closed-loop transfer function

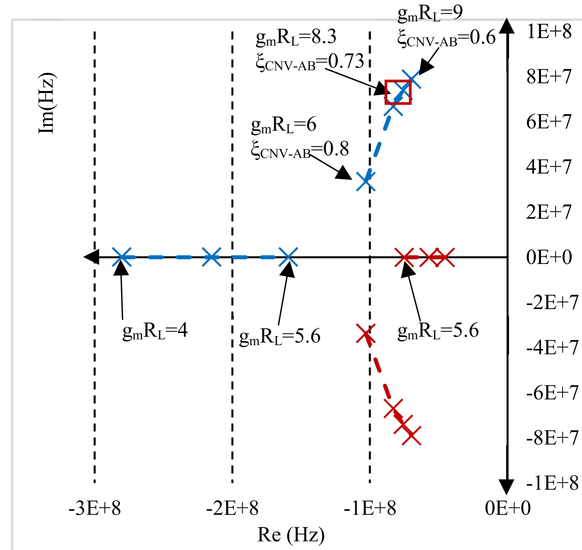

Fig. 4. Root locus of poles of CNV-AB-VF [10] for varying open-loop gain $A_{\text{OL}} = g_m R_L$.

$G_{\text{CL}}(s) = (V_{\text{Out}}/V_{\text{in}})(s)$ of the CNV-AB-VF is given by

$$G_{\text{CL}}(s) = \frac{(a/C_X C_L)(1 + sC_X g_{m1}/a)}{s^2 + 2\xi_{\text{CNV-AB}}\omega_{n\text{CNV-AB}} s + \omega^2_{n\text{CNV-AB}}} \quad (1)$$

where

$$\begin{aligned} a &= (G_L g_{m1} + g_{m1} g_{m2}) \\ g_{m1b} &= (g_{m1} + g_{mb}) \\ 2\xi_{\text{CNV-AB}}\omega_{n\text{CNV-AB}} &= (g_{m1b}/C_L) + (G_L/C_X) \\ \omega^2_{n\text{CNV-AB}} &= (g_{m1b} G_L/C_X C_L) + (g_{m1b} g_{m2}/C_X C_L) \\ &= (g_{m1b}/C_X C_L)(G_L + g_{m2}). \end{aligned}$$

In this analysis, the zero created by C_{gs} of M_1 is ignored. The zero has a frequency $f_{Z\text{cgs1}} = (1/2\pi)(g_{m1}/C_{\text{gs1}})$ that has a very high value (~GHz) and thus does not affect the response in the range of operation of the follower. Substituting $g_{m2} = g_{m1} = g_m$ in (1), it can be observed that the closed-loop gain G_{CL} has a zero at $\omega_Z = (G_L + g_m)/C_X$ and two poles. As the capacitance at node V_X, given by C_X, is very small, this zero is also at very high frequency. Hence, the effect of this zero is assumed to be negligible. The poles can be either real or complex conjugate, depending on the value of the dc open-loop gain $A_{\text{OL}} = g_m R_L$ of the negative feedback loop. For example, a root locus plot of the poles of G_{CL} as a function of $g_m R_L$ is shown in Fig. 4. It is obtained for a typical design in the 130-nm CMOS technology with $I_B = 50\ \mu$A, dual supply voltages of ± 0.6 V, $C_L = 20$ pF, and transistor dimensions $W/L = 15/0.15$ (μm). The forgoing parameters result in $g_m = 836\ \mu$A/V, $r_o = 25$ kΩ, and $C_x \approx 0.1$ pF. This plot reveals that for values $g_m R_L < 6$, the poles are on the negative real axis. As the gain $g_m R_L$ continues to increase, the poles move toward each other and become complex conjugate (for example for the values of $g_m R_L > 6$) and the BW can be obtained by [11]

$$\text{BW} = \omega_{3\,\text{dB}} = \omega_n \sqrt{(1 - 2\zeta^2) + \sqrt{(4\xi^4 - 4\xi^2 + 2)}}. \quad (2)$$

This article has been accepted for inclusion in a future issue of this journal. Content is final as presented, with the exception of pagination.

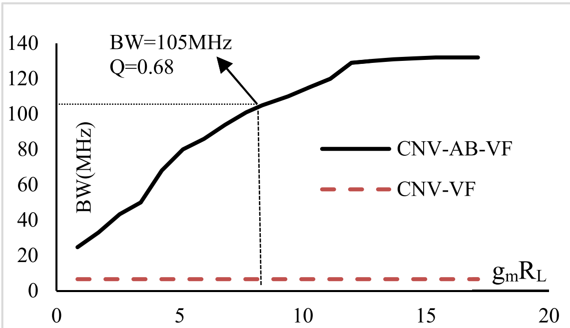

Fig. 5. BW of CNV-AB-VF and CNV-VF as a function of $g_m R_L$.

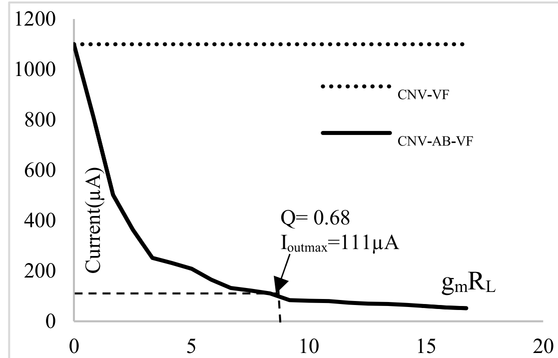

Fig. 6. Maximum positive output current for CNV-VF and CNV-AB-VF as a function of $g_m R_L$.

For the CNV-AB-VF, ξ and ω_n are given, respectively, by

$$\xi_{\text{CNV-AB}} = [(g_{m1b}/C_L) + (G_L/C_X)]/2\omega_{n\text{CNV-AB}} = 1/2Q \tag{3}$$

$$\omega_{n\text{CNV-AB}} = \sqrt{(G_L + g_m)(g_{m1b}/(C_X C_L))}. \tag{4}$$

As $g_m R_L$ increases, the BW (see Fig. 5) and the Q factor increase (the damping ratio ζ decreases as shown in Fig. 4). To avoid peaking in the frequency response (or overshoot in the transient response), values $Q < 0.707$ or $\zeta > 0.707$ need to be selected. For $\zeta = 0.707$, the maximum BW $= \omega_n/2\pi$ without overshoot in the transient response is achieved. In this example, from the root locus, a value $g_m R_L = 8.3$ leads to $\xi_{\text{CNV}-\text{AB}} = 0.73$ and $Q = 0.68$. Thus, the corresponding BW can be obtained from (2) inserting the values of $\xi = 0.73$ and ω_n from (4). For $g_m = 836\ \mu\text{A/V}^2$, $g_{m1b} = g_m(1+\eta)$, $\eta = 0.2$ [12], $C_X = 0.1$ pF, $C_L = 20$ pF, and $R_L = 10$ kΩ, the BW is $\text{BW}_{\text{CNV}-\text{AB}-\text{VF}} = 105$ MHz, which is 16 times higher than the BW of the CNV-VF given by $BW_{CNV-VF} = g_m/2\pi C_L = 6.6$ MHz. Fig. 5 shows that the BW continues to increase until $g_m R_L = 16$. However, it is not desirable to increase $g_m R_L$ for the values of $Q > 0.707$ in order to avoid overshoot in the transient response and peaking in the frequency response. A drawback of the CNV-AB-VF is that when R_L increases even for values $Q < 0.707$, the voltage drop across R_L increases and causes V_X and V_{DS} of the M_1 transistor to decrease. This leads to a significant decrease in the maximum positive output current and in turn to a decrease in the positive SR of the circuit. Fig. 6 shows the maximum positive output current of the CNV-AB-VF as a function of R_L. It can be observed that the maximum output current decreases by a factor of 10 from 1100 μA for $g_m R_L = 0$ to 111 μA for $g_m R_L = 8.3$ and $Q = 0.68$. The PRP-AB-VF overcomes this problem. The small signal analysis of the PRP-AB-VF is discussed in Section IV.

IV. Small Signal Analysis of Proposed Class AB VF

The proposed circuit shown in Fig. 2(c) can achieve simultaneously large positive and negative SRs and essentially an improved BW. This circuit has the same quiescent power dissipation as the CNV-VF and as the CNV-AB-VF. It incorporates just one additional transistor $M_{1\text{AB}}$ that acts as a CNV-VF. This transistor can provide a large positive output current independent of the value of R_L that is used to control the enhancement of the BW and the negative SR. The small signal analysis of the proposed circuit is discussed in detail in this section. The ac equivalent circuit of the PRP-AB-VF for $f > f_o$ is shown in Fig. 7. The proposed VF is designed for relatively large capacitive loads C_L that satisfy $C_L \gg C_{\text{gs}}$. Since the PRP-AB-VF was not intended for applications in oscillators where negative input resistance of the follower is important [13], [14], the effect of C_{gs} is ignored in the small signal analysis. As the dimension (W/L) of all the transistors in Fig. 2(c) are equal, and the total bias current of the circuit is I_B, the quiescent current of M_1 and $M_{1\text{AB}}$ is $I_B/2$. In the PRP-AB-VF, the sizes of all the transistors are the same as in CNV-VF and CNV-AB-VF. This maintains equal power dissipation in the three VF circuits. Hence, if transistors operate in a strong inversion, the transconductance gains $g_{m1\text{P}}$ and $g_{m1\text{AB}}$ of $M_{1\text{P}}$ and $M_{1\text{AB}}$ in the proposed circuit are a factor $1/\sqrt{2}$ times smaller than the transconductance gain of M_1 of the CNV-VF (see Fig. 1) and of the CNV-AB-VF [see Fig. 2(b)]. Thus, $g_{m1\text{P}} = g_{m1\text{AB}} = g_m/\sqrt{2}$ and $g_{m1\text{Pb}} = g_{m1\text{ABb}} = (1+\eta)\ g_m/\sqrt{2} = (1.2)g_m/\sqrt{2}$. Transistors M_2 and M_{2p} in Fig. 2(b) and (c) carry equal bias currents (I_B) and have identical dimensions in order to keep the equal power dissipation as the CNV-VF and the CNV-AB-VF circuits. Hence, their transconductance gains are equal ($g_{m2} = g_{m2\text{P}} = g_m$) and both the CNV-AB-VF and the PRP-AB-VF have equal open-loop gain $A_{\text{OL}} = g_m R_L$. Hence, the closed-loop transfer function ($G_{\text{CLP}} = V_{\text{Out}}/V_{\text{in}}$) of the proposed VF is given by (5). This transfer function has a zero and two poles. As in Section III, a very high-frequency zero created by C_{gs} of M_1 is ignored

$$G_{\text{CLP}}(s) = \frac{(a_{\text{PRP}}/C_X C_L)(1 + \sqrt{2} s C_x g_m / a_{\text{PRP}})}{(s^2 + 2\xi\omega_{n\text{PRP}} s + \omega_{n\text{PRP}}^2)} \tag{5}$$

where

$$a_{\text{PRP}} = \left(G_L\sqrt{2}g_m + g_m^2/\sqrt{2}\right)$$
$$2\xi_{\text{PRP}}\omega_{n\text{PRP}} = (1.2\sqrt{2}g_m/C_L + G_L/C_X)$$
$$\omega_{n\text{PRP}}^2 = \left(1.2\sqrt{2}g_m G_L + g_m^2/\sqrt{2}\right)/(C_X C_L).$$

Here, it is assumed that $G_L = 1/R_L$, C_{gs} and $C_x \ll C_L$, $g_m \gg g_{\text{o}}$, and $G_L > g_{\text{o}}$. The zero of the circuit associated with

This article has been accepted for inclusion in a future issue of this journal. Content is final as presented, with the exception of pagination.

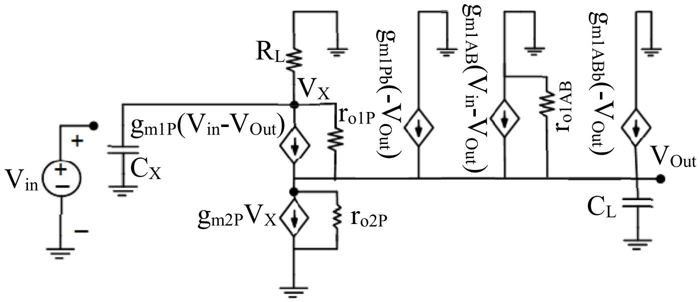

Fig. 7. Small signal model of PRP-AB-VF.

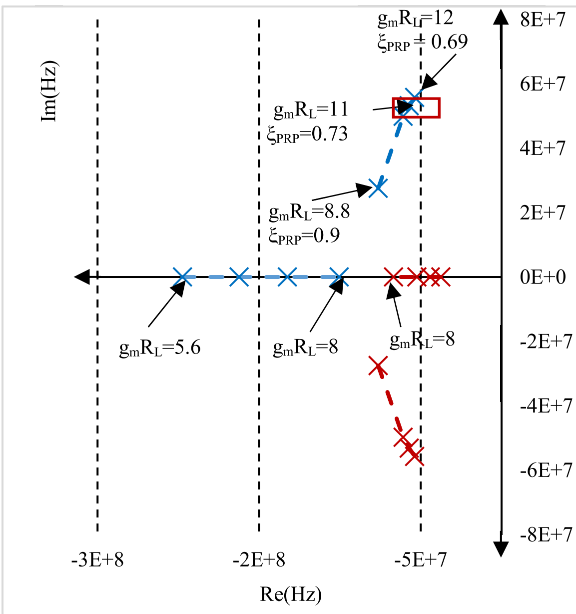

Fig. 8. Root locus of PRP-AB-VF as a function of open-loop gain $A_{\mathrm{OL}} = g_m R_L$.

node V_X is given by $\omega_{\mathrm{ZPRP}} = (G_L/C_X) + (g_m/2C_X)$. As in the previous circuit, C_X is very small, and for this reason, ω_{ZPRP} also remains at high frequency and does not have a significant effect on the transfer function. The damping ratio ξ_{PRP} and $\omega_{n\mathrm{PRP}}$ can be expressed, respectively, as shown in

$$\xi_{\mathrm{PRP}} = (1.2\sqrt{2}g_m/C_L + G_L/C_X)/(2\omega_{n\mathrm{PRP}}) \qquad (6)$$

$$\omega_{n\mathrm{PRP}} = \sqrt{\left(1.2\sqrt{2}g_m G_L + g_m^2/\sqrt{2}\right)/C_X C_L}. \qquad (7)$$

The root locus of the proposed VF is given in Fig. 8 for similar conditions as in Section III: bias current $I_B = 50$-μA, ± 0.6-V supply voltage, and equal W/L (15/0.15) (in μm) of all transistors.

Similar as in the CNV-AB-VF with increasing loop gain $g_m R_L$, the poles move toward each other, and after $g_m R_L$ reaches a certain value, they become complex conjugate. In the design example, poles become complex conjugate for open-loop gains $g_m R_L > 8$, as shown in Fig. 8. When poles are complex conjugates, the BW of the PRP-AB-VF can be obtained from (2). For the proposed circuit when there is no overshoot in the transient response, the value of $\xi_{\mathrm{PRP}} = 0.73$,

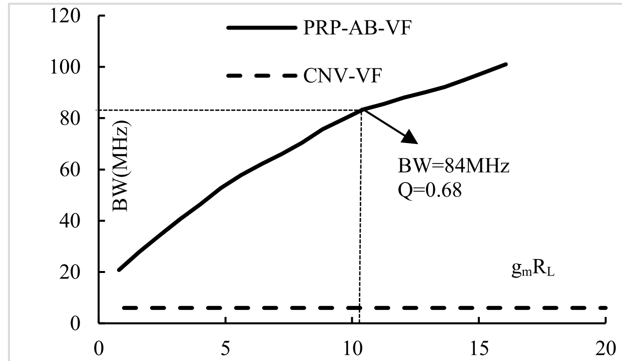

Fig. 9. BW of PRP-AB-VF and CNV-VF as a function of $g_m R_L$.

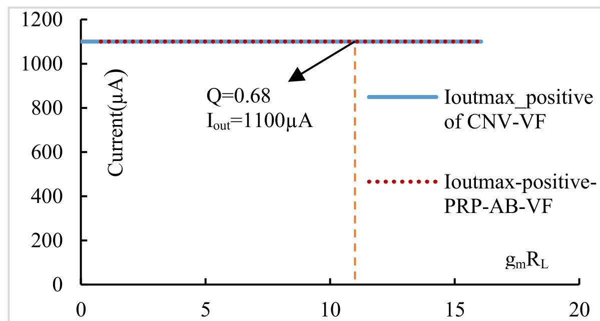

Fig. 10. Maximum positive output current PRP-AB-VF and CNV-VF for varying $g_m R_L$.

$g_m R_L = 11$, and $Q = 0.68$. In this condition, the maximum BW without peaking in the frequency response is $\mathrm{BW}_{\mathrm{PRP-AB-VF}} = 0.96\omega_{n\mathrm{PRP}}/2\pi$. The numerical value of the BW can be determined by inserting values of ξ_{PRP} and $\omega_{n\mathrm{PRP}}$ into (2). The value of $\omega_{n\mathrm{PRP}}$ can be calculated by inserting the values $g_m = 836$ μA/V^2, $C_X = 0.1$ pF, $C_L = 20$ pF, and $R_L = 13$ kΩ in (7). Thus, the BW of PRP-AB-VF for $\xi_{\mathrm{PRP}} = 0.73$ is 84 MHz, which is 12 times higher than the BW of the CNV-VF and allows a large positive output current independent of $g_m R_L$ as shown in Figs. 9 and 10. Fig. 11 shows the simulation of the input impedance of the PRP-AB-VF and CNV- VF. It can be observed that the input impedance has a slope of -20 dB and $-90°$ phase from 1 kHz to 25 MHz. This implies that the input impedance is mainly capacitive for frequencies from 1 kHz to 25 MHz. The input impedance corresponds to an extremely large resistance $R_{\mathrm{in}} \sim 400$ GΩ in parallel with an extremely small capacitor $C_{\mathrm{in}} \approx 7$ fF over a very wide BW. Hence, it will have a minimal loading effect on the response of the circuit where it will be used as a buffer. The analytical expression of the input impedance is given in the Appendix.

V. Comparison of Followers

In this section, the response of the proposed VF is compared with the CNV-AB-VF to demonstrate the significant advantage of the former predicted by the small signal analysis and simulation results. The experimental verification results are given in Section VII. The effective speed of the VF depends on both the BW and the SR. The BW determines the exponential

This article has been accepted for inclusion in a future issue of this journal. Content is final as presented, with the exception of pagination.

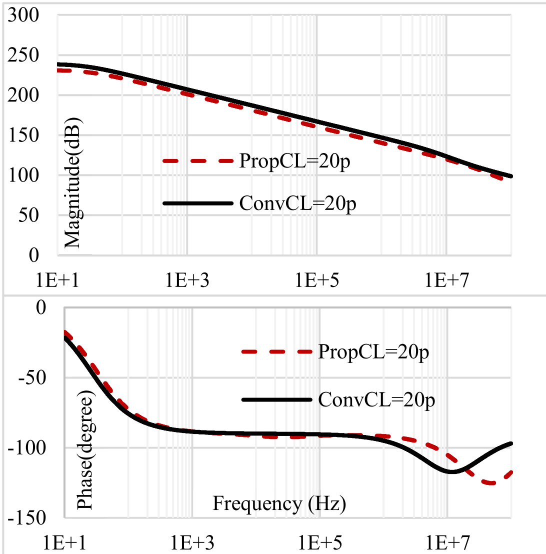

Fig. 11. Input impedance magnitude and phase for $C_L = 20$ pF.

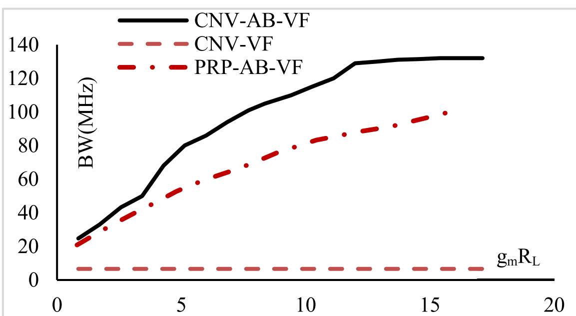

Fig. 12. Comparison of BW of VFs as a function of $g_m R_L$.

component of the settling time, while the SR determines the linear component of the settling time. To reduce the settling time, both the BW and the SR need to be improved simultaneously. It is also desirable to have approximately equal maximum positive and negative output currents in order to have symmetrical SRs. This is important, since as indicated Section I, the minimum of the positive and negative SRs determines the SR of the circuit. From Fig. 12, it is observed that increasing R_L $(g_m R_L)$ provides large BW enhancement for the CNV-AB-VF with respect to class A CNV-VF in Fig. 1. However, Fig. 13 shows that despite providing a larger negative output current, the CNV-AB-VF has very low positive output current for a large R_L value, which degrades the positive SR given by $\text{SR}^+ = dV_{\text{Out}}/dt = I_{\text{Out}}^+/C_L$. The output current can be expressed as $I_{\text{Out}}^+ = \text{SR} \cdot C_L$. The PRP-AB-VF provides a consistently high maximum positive (and negative) output current for all the values of $R_L(g_m R_L)$ with the same bias current. This is because of the transistor $M_{1\text{AB}}$ in Fig. 2(c), which acts as a CNV-VF and can provide a large maximum positive output current independent on the value of R_L. For $g_m R_L = 11$ $(\xi_{\text{PRP}} = 0.73)$, the positive and negative currents are equal in the PRP-AB-VF. Thus, almost symmetric SR can be obtained from the proposed VF. Fig. 14(a) and (b)

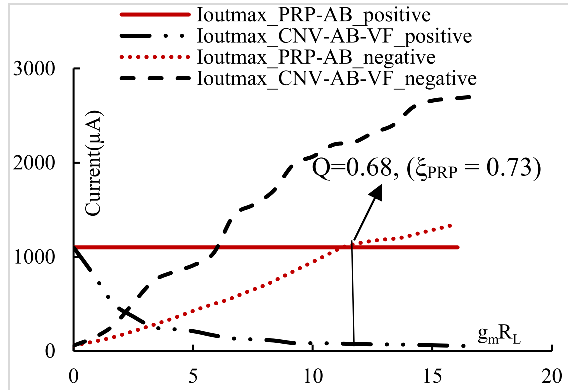

Fig. 13. Maximum positive and negative current of PRP-AB-VF and CNV-AB-VF for varying $g_m R_L$.

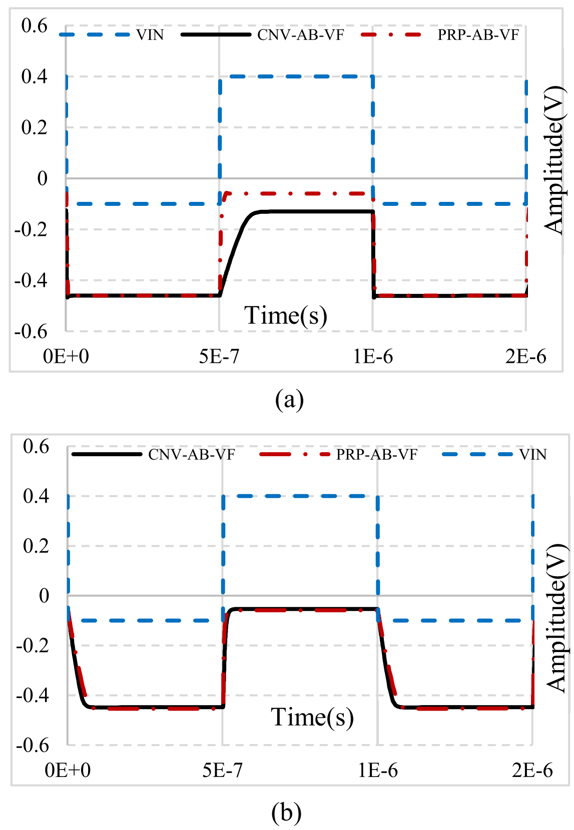

Fig. 14. Transient response of CNV-AB-VF and PRP-AB-VF for (a) $R_L = 13$ kΩ and (b) $R_L = 1$ kΩ.

shows the transient responses of the CNV-AB-VF and the PRP-AB-VF for $R_L = 13$ kΩ and $R_L = 1$ kΩ, respectively. These are for a 500-mV peak-to-peak 1-MHz input square pulse, and $C_L = 20$ pF. Fig. 14 depicts that for large R_L values, the positive SR of CNV-AB-VF deteriorates while both the positive and negative SRs of the PRP-AB-VF remain high, whereas for small $R_L = 1$ kΩ values, as expected, the negative SR of both the circuits deteriorates. This validates that the simultaneous improvement of positive and negative SRs and BW is not possible in the CNV-AB-VF.

This article has been accepted for inclusion in a future issue of this journal. Content is final as presented, with the exception of pagination.

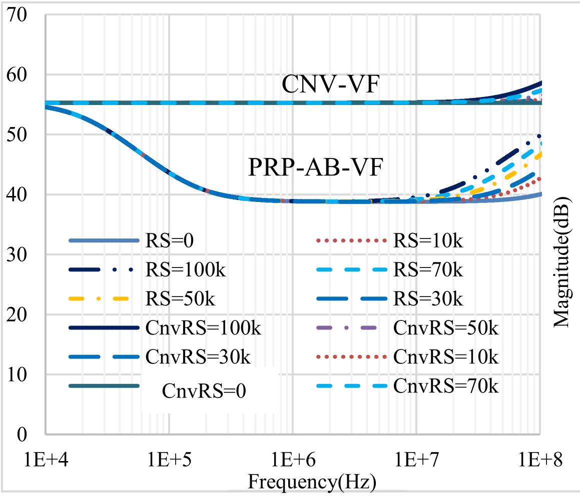

Fig. 15. Simulated output impedance of PRP-AB-VF and CNV-VF for nonideal source.

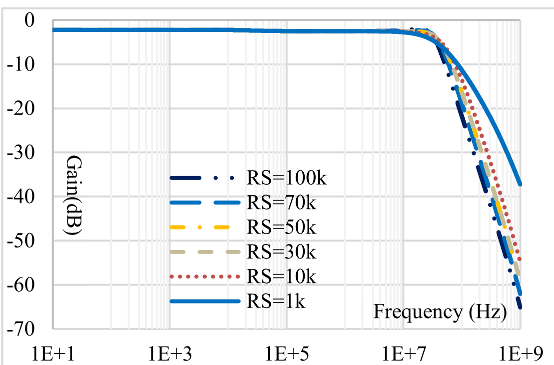

Fig. 16. Frequency response of the PRP-AB-VF for nonideal source where R_S is parameterized from 1 to 100 kΩ for $C_L = 50$ pF.

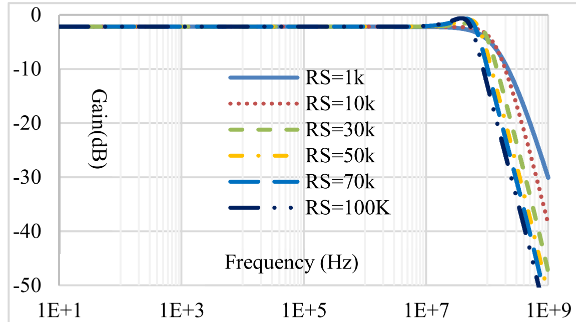

Fig. 17. Frequency response of the PRP-AB-VF for nonideal source with R_S parameterized from 1 to 100 kΩ for $C_L = 10$ pF.

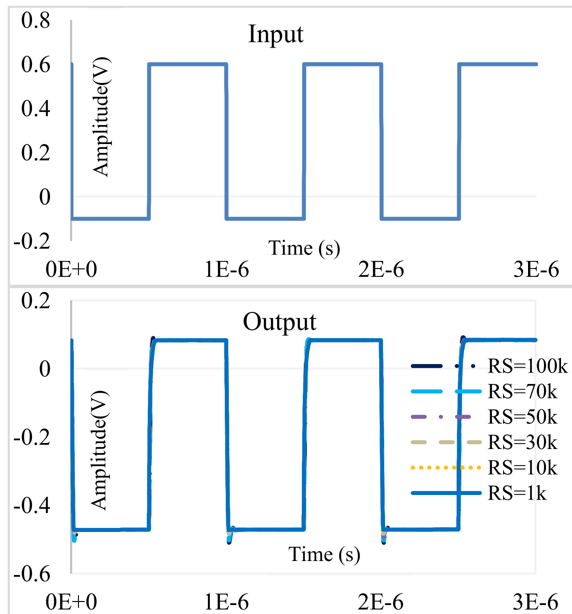

Fig. 18. Transient response of the PRP-AB-VF for nonideal source with R_S parameterized from 1 to 100 kΩ for $C_L = 50$ pF.

From Figs. 4 and 8, it is observed that for increasing $g_m R_L$, the complex poles of the previously reported CNV-AB-VF are closer to the imaginary axis than the PRP-AB-VF. Thus, the CNV-AB-VF has a lower damping ratio (ξ) than the proposed one. The lower damping ratio leads to a higher overshoot in the transient response of the circuit. The damping ratio (ξ) for the CNV-AB-VF is less than 0.7 for an open-loop gain of 9, whereas the damping ratio for the proposed VF is less than 0.7 for an open-loop gain of 12. Hence, the open-loop gain of the PRP-AB-VF can be increased to a value $g_m R_L = 11$, without overshoot in the transient response. Consequently, it will help to increase even further the BW of the circuit keeping symmetrical and improved SR.

VI. Proposed AB-VF With Nonideal Source

The application considered in this paper for the proposed VF is to serve as a buffer for amplifiers. The internal resistance of the signal source R_S and the C_{gs1P} neglected in the derivation of Section IV might affect the response of the follower as reported in [13]–[15]. In this section, we showed that R_S and C_{gs1P} have negligible effect in the transient and magnitude response of the PRP-AB-VF over a wide range of R_S values for the range of C_L values considered here. The simulated output impedance of PRP-AB-VF and CNV-VF, magnitude, and transient responses of the PRP-AB-VF are shown in Figs. 15–19. The simulations have been performed considering a nonideal source to evaluate the effect of a nonideal source with nonzero internal resistance R_S. The values of R_S were parameterized from 1 to 100 kΩ. From Fig. 15, it can be observed that the CNV-VF has a constant 630-Ω output impedance, whereas the PRP-AB-VF has 100-Ω output impedance over the frequency range of 226 kHz to 50 MHz for the ideal source. The output impedance starts to decrease after 226 kHz because of the cutoff frequency $f_0 = 1/R_{\text{large}} C_{\text{BAT}}$ of the combination of R_{large} and C_{BAT}, which provides the dynamic class AB operation. From Fig. 15, it can be asserted that as the frequency increases, the value of Z_{Out} approaches R_S as expected [12]. The analytical expression of the output impedance is given in the Appendix. Regarding the magnitude response from Fig. 16, it can be asserted that the PRP-AB-VF has no peaking in the frequency response up to source resistances with value $R_S = 100$ kΩ when $C_L = 50$ pF.

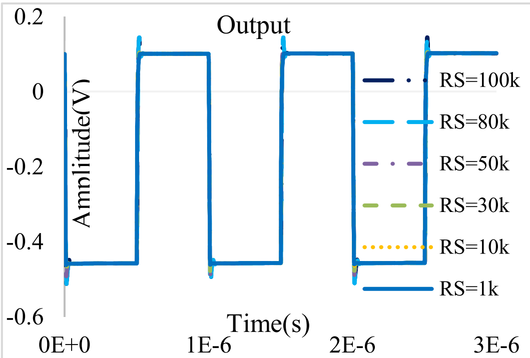

Fig. 19. Transient response of the PRP-AB-VF for nonideal source where R_S parameterized from 1 to 100 kΩ for C_L = 10 pF.

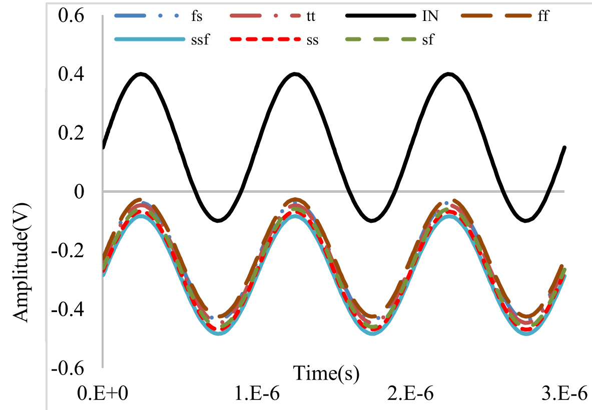

Fig. 20. Simulated transient response of PRP-AB-VF at six different corners for 1-MHz 500-mV peak-to-peak sinusoidal signal.

TABLE I

THD AT SIX DIFFERENT CORNERS AND THEIR SDS

Corner	THD PRP-AB-VF (%)	S.D.	THD CNV-AB-VF (%)	S.D.	THD CNV-VF (%)	S.D.
tt	0.27	0.03	0.52	0.03	1.54	0.16
fs	0.22		0.54		1.50	
sf	0.32		0.53		1.64	
ss	0.26		0.55		1.72	
ff	0.28		0.51		1.42	
ssf	0.25		0.58		1.86	

However, for the lower value of C_L, it has moderate peaking for $R_S = 70$ kΩ in Fig. 17. Figs. 18 and 19 show the transient response of the PRP-AB-VF for C_L = 50 and 10 pF at a 1-MHz square pulse generated by a nonideal signal source. It can be seen that for a larger source resistance, the overshoots in the transient response become lower with the increase in C_L value. Hence, an amplifier with a relatively large output impedance can be interfaced with the PRP-AB-VF for load capacitances with values $C_L > 10$ pF without introducing significant peaking. The small signal model of PRP-AB-VF with nonideal source and C_{gs1P} is given in the Appendix.

VII. EXPERIMENTAL/SIMULATION RESULTS

The PRP-AB-VF, CNV-AB-VF, and CNV-VF were fabricated in a 0.13-μm CMOS n-well process with 15/0.15-unit transistor size (in μm), R_{large} = 500 kΩ, and C_{BAT} = 2-pF capacitor. The CNV-AB-VF was fabricated with R_L = 1 kΩ ($g_m R_L = 0.8$). A value of R_L = 13 kΩ ($g_m R_L = 11$) was used for the PRP-AB-VF. This value leads to a maximum BW and symmetrical SR also, as explained in Section V. The circuits were tested and simulated with R_S = 50 Ω, a bias current I_B = 50 μA, dual supply voltages ±0.6 V, and C_L = 50 pF. The load resistance R_L of the proposed VF is implemented with a PMOS transistor operated in the triode region with dimensions (in μm) 0.9/0.18 with the gate connected to a bias voltage $V_{\mathrm{bias}} = -100$ mV. Fig. 20 shows the simulated transient response of the PRP-AB-VF for 500-mv peak-to-peak 1-MHz input sinusoidal signal at six different corners.

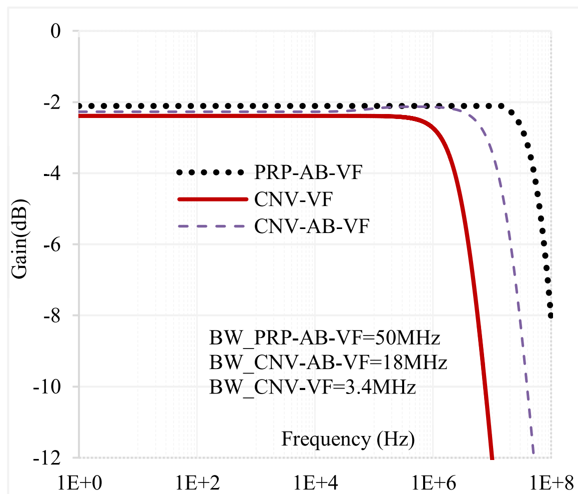

Fig. 21. Experimental frequency response of PRP-AB-VF, CNV-AB-VF, and CNV-VF for 50-pF load capacitance.

Table I shows the simulated total harmonic distortion (THD) of the PRP-AB-VF, the CNV-AB-VF, and the CNV-VF at six different corners. The standard deviations (SDs) of the THD at six different corners are also shown in Table I for CNV-VF, CNV-AB-VF, and PRP-AB-VF. The THD of the proposed VF is lower than that of the CNV-VF and of the CNV-AB-VF for 500-mv peak-to-peak 1-MHz sinusoidal input signal, as it has a higher SR than previously stated VFs.

Fig. 21 shows the experimental frequency response of the PRP-AB-VF, CNV-AB-VF, and CNV-VF. Fig. 22 shows the experimental transient response of the CNV-VF, CNV-AB-VF, and the PRP-AB-VF for a 1-MHz (500-mV peak-to-peak amplitude) input pulse. The PRP-AB-VF has an experimental BW value $\mathrm{BW}_{\mathrm{PRP-AB-VF}}$ = 50 MHz with C_L = 50 pF, while the BW of the CNV-AB-VF is $\mathrm{BW}_{\mathrm{CNV-AB-VF}}$ = 18 MHz. The BW of CNV-VF is 3.4 MHz. From the experimental transient response, it can be observed that the PRP-AB-VF has the highest negative SR compared with the CNV-AB-VF.

At the value of R_L = 1 kΩ ($g_m R_L = 0.8$), the CNV-AB-VF has a maximum positive output current and a low negative current [shown in Figs. 13 and 14(b)] and the BW

TABLE II
PERFORMANCE COMPARISON OF CNV-VF, CNV-AB-VF, AND PRP-AB-VF WITH OTHER CLASS AB VFS IN LITERATURE

Parameter	CNV-VF Fig.1	Ref [4]	Ref [10] (CNV-AB-VF) Fig.2b		Ref [16]		Ref [17]		Ref [18]	Ref[6]	Ref [19] Fig.2c	This work (PRP-AB-VF) Fig. 2c
	Exp	Exp AB#1-3	Exp In Ref [6]	Exp In this work	Sim	Simulated by authors	Exp	Simulated by authors	Exp	Exp	Exp	Exp
Process technology	CMOS 0.13μm	CMOS 0.5 μm	ALD1106 Tran. Array	CMOS 0.13μm	CMOS 0.5 μm	CMOS 0.13 μm	CMOS 0.35 μm	CMOS 0.13 μm	CMOS 0.35 μm	CMOS 0.18 μm	CMOS 0.5 μm	CMOS 0.13μm
Supply (V)	±0.6	±1.65	2.7	±0.6	±1.5	±0.6	3	±0.6	3.3	±0.9	±1.65	±0.6
I_{Bias} (μA)	50	10	55	50	30	50	10	50	500	30	10	50
Load Cap (pF)	50	30	280	50	10	50	20	50	12	50	30	50
BW(MHz)	3.4	8.4-13.4	2	18	70	46	5.8	6.16	87	32	13.1	50
I_{out}^{Max+} (mA)	0.95	0.6-0.87	0.92	0.9	0.850	2.1	1.62	3.1	2.4	1.3	0.75	0.975
I_{out}^{Max-} (mA)	0.075	0.51-1.05	0.54	0.16	0.525	1.7	1.67	3.2	NA	1.01	NA	1.33
SR^+ (V/μS)	19	20-29	3.75	18	85	60	79.4	62	200	25.6	25	19.5
SR^-(V/μS)	1.5	17-35	1.82	3.2	52.5	35	83.6	64	NA	20.1	NA	26.75
Input noise spectral density @1MHz (nV/√Hz)	18 (simulated)	30-55	NA	16 (simulated)	NA	NA	NA	NA	NA	NA	40	16 (simulated)
Silicon area(mm^2)	0.002	0.014-0.025	NA	0.0067	NA	NA	0.014	NA	0.0097	0.013	0.011	0.0074
Quiescent power P^Q(μWatt)	60	165-198	148.5	60	198	168	243	486	3300	229	99	60
$FOM_{CE}= I_{outMAX}/I_{Qtotal}$	1.5	10-14.5	9.8	3.2	7.5	12	20	8	2.4	8	25	19.5
$FOM_{BW}= (BW * C_L)/P^Q$ [(MHz)pF]/ μW	2.8	1.5-2.03	3.77	15	3.53	13	0.47	0.62	0.32	7	3.96	41.6
$FOM_{GLB}= \sqrt{FOM_{BW}FOM_{CE}}$	2.04	3.87-5.43	6.07	6.9	5.14	12.8	3.06	2.22	0.87	7.5	9.94	28

is also less than the PRP-AB-VF (shown in Fig. 12). Hence, the experimental transient and frequency response validate the theoretical claim.

The simulated input noise spectral density of CNV-VF, CNV-AB-VF, and PRP-AB-VF is given in Table II. The PRP-AB-VF has 16-nV/$\sqrt{}$Hz input noise spectral density. Fig. 23 shows settling the response of the PRP-AB-VF at different capacitive loads. A 50-mV amplitude and 1-MHz step signal is applied at the input of the PRP-AB-VF to observe the settling performance of the PRP-AB-VF. For C_L of 50 pF, the settling time is 22.4 ns (2% of its final value). From Fig. 23, it can be observed that the transient response has a peak overshoot for a load $C_L = 5$ pF. Hence, for that load, the damping ratio ξ is less than 0.7. It can be asserted that from the settling time response of the PRP-AB-VF, the minimum load capacitance C_L of 10 pF it can drive without overshoot in the output response. Fig. 24 shows the simulated transient responses of the CNV-VF, CNV-AB-VF, PRP-AB-VF, and FVF [9] for an input triangular pulse with 900-mV peak-to-peak amplitude and 100-kHz frequency. This exhibits that the AB-FVF of [9] has a serious swing limitation. The PRP-AB-VF has 900-mV output swing, whereas FVF [9] provides only 373-mV output swing.

Table II compares the performance parameters of the conventional, PRP-AB-VF, and several recently published class

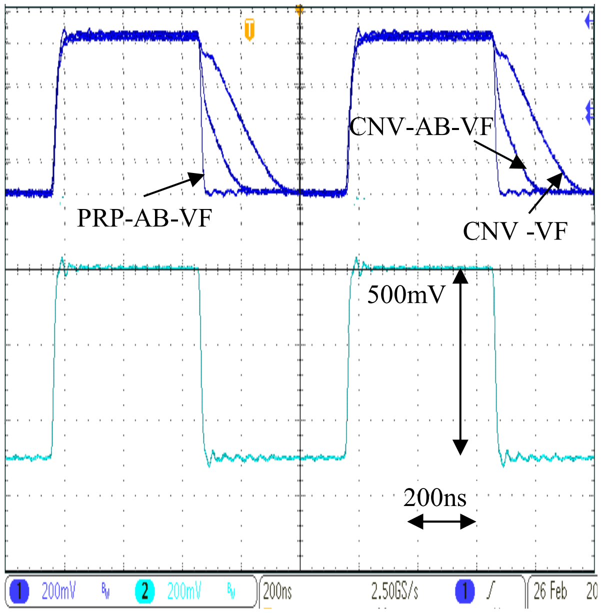

Fig. 22. Experimental transient response of PRP-AB-VF, CNV-AB-VF, and CNV-VF for 500-mV amplitude pulse at 1 MHz.

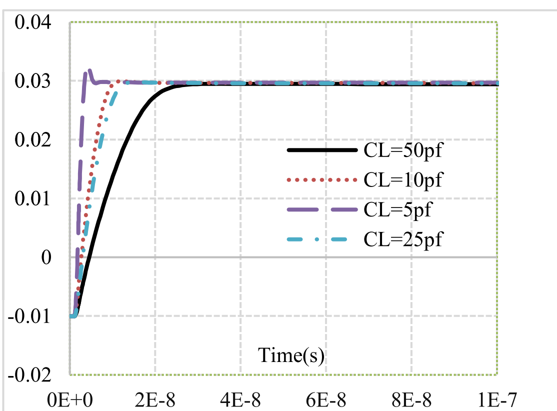

Fig. 23. Settling time for different load capacitances for PRP-AB-VF for 50-mV amplitude square pulse of 1 MHz.

AB buffers [4], [6], [10], [16]–[19]. "Exp" and "Sim" refer to the experimental and simulation results, respectively. The implementation technology and supply voltage can have a significant effect on the performance of a circuit. In this paper, references [16] and [17] were simulated by authors in CMOS 0.13-μm technology for a fair comparison. From Table II, it can be observed that the current efficiency figure of merit ($\mathrm{FOM_{CE}}$) of the proposed VF is comparable with [17] in the CMOS 0.35-μm technology. However, the small signal figure of merit $\mathrm{FOM_{BW}}$ of the proposed VF is more than 67 times higher than that of [17] in both the technologies and $\mathrm{FOM_{CE}}$ is less in the 0.13-μm technology. Though $\mathrm{FOM_{CE}}$ of [19] is also 1.2 times higher than that of the PRP-AB-VF, yet $\mathrm{FOM_{BW}}$ of PRP-AB-VF is 10 times higher than in [19]. The geometric mean of the two figures of merit has been calculated and used as a global speed figure of merit ($\mathrm{FOM_{GLB}} = (\mathrm{FOM_{BW}}\mathrm{FOM_{CE}})^{1/2}$) to compare recently reported buffers and the PRP-AB-VF. The PRP-AB-VF has a

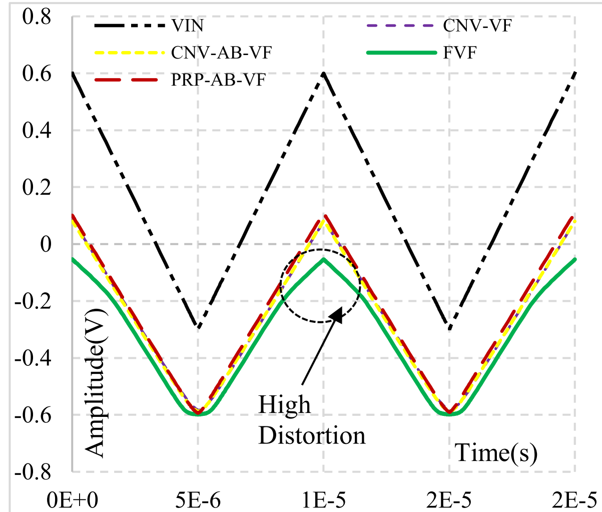

Fig. 24. Input/output range of the VFs.

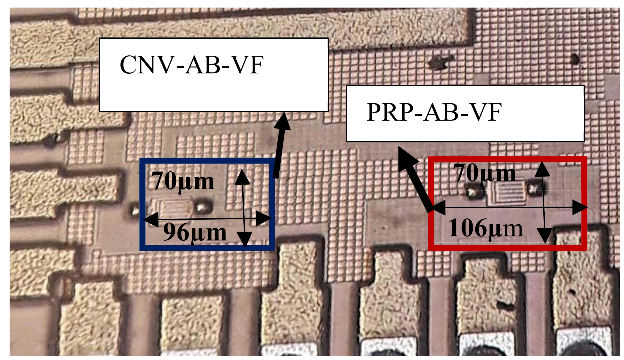

Fig. 25. Chip micrograph of CNV-AB-VF and PRP-AB-VF.

global speed figure of merit $\mathrm{FOM_{GLB}} = 28$, which is the highest among all circuits. The chip micrograph of the CNV-AB-VF and the PRP-AB-VF is shown in Fig. 25. The silicon area consumed by the PRP-AB-VF is 0.0074 mm^2, and the CNV-AB-VF is 0.0067 mm^2. The CNV-VF occupied 0.002 mm^2 of the Si area. The proposed circuit has four times higher $\mathrm{FOM_{GLB}}$, six times higher $\mathrm{FOM_{CE}}$, and three times higher $\mathrm{FOM_{BW}}$ compared with the CNV-AB-VF at the expense of only 10% more Si area than the CNV-AB-VF. Compared with the CNV-VF, the PRP-AB-VF provides 13 times higher $\mathrm{FOM_{CE}}$, 14.8 times higher $\mathrm{FOM_{BW}}$, and 13.8 times higher $\mathrm{FOM_{GLB}}$.

VIII. Conclusion

A simple modification to a CNV-AB-VF has been shown to significantly improve the positive and negative SRs and the BW, with the same power dissipation and a small additional silicon area with respect to the CNV-VF and the CNV-AB-VF. This has been demonstrated by performing an analytical and experimental comparison of the proposed circuit to the above-mentioned VFs. It has been shown that the proposed circuit has the highest global figure of merit of all the VFs reported in the literature. It has 13 times higher current efficiency and 14.8 times higher $\mathrm{FOM_{BW}}$ than the CNV-VF with the same power dissipation.

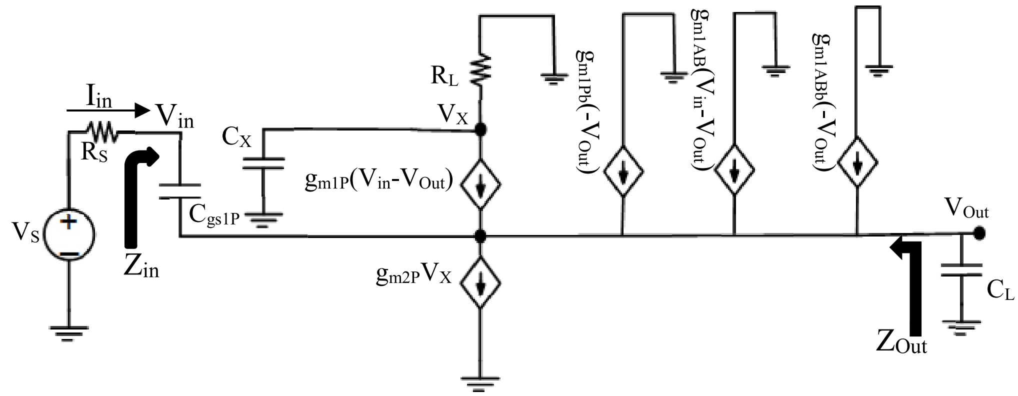

Fig. 26. Small signal model of the proposed VF considering $C_{\text{gs}1P}$ and nonideal source.

APPENDIX
EXPRESSION FOR INPUT IMPEDANCE, OUTPUT IMPEDANCE, AND Q OF PROPOSED AB-VF

The PRP-AB-VF can be used as an oscillator for low C_L values. In this case, C_L might not satisfy the condition $C_L \gg Cgs$ and the small signal model in Fig. 26 will be used considering $g_m \gg g_o$. From this model, the input impedance Z_{in} of the follower is given by (1A). Z_{in} has a real component that corresponds to a negative frequency-dependent resistance which is important for oscillator applications

$$Z_{\text{in}}(\omega) \approx -\frac{g''_{m1\text{P}}}{(\omega^2 C_L C_{\text{gs1P}})} - \frac{g_{m1\text{P}} g_{m2P}(\omega^2 G_L C_{\text{gs1P}} C_L)}{(-\omega^2 C_{\text{gs1P}} C_L G_L)^2 + (\omega^3 C_X C_{\text{gs1P}} C_L)^2} + \frac{(C_L + C_{\text{gs1P}})}{j(\omega C_L C_{\text{gs1P}})}. \quad \text{(1A)}$$

$V_{\text{Out}}/V_{\text{S}}$ is a second-order transfer function (not shown here) with Q given by (2A), as shown at the bottom of this page.

Neglecting body effect and assuming $g_0 \ll g_m$, Z_{Out} is given by (3A), as shown at the bottom of this page.

Here, $g''_{m1\text{p}} = g_{m1} + g_{m1\text{P}}$ and $1.2g''_{m1\text{P}} = (1+\eta)g''_{m1\text{P}}$ where $\eta = 0.2$ is the body effect coefficient. From the equation of Z_{Out}, it can be observed that at higher frequencies, the output impedance Z_{Out} is $Z_{\text{Out}} \sim R_{\text{S}}$ which is consistent with simulations shown in Fig. 15.

REFERENCES

[1] R. G. Carvajal *et al.*, "The flipped voltage follower: A useful cell for low-voltage low-power circuit design," *IEEE Trans. Circuits Syst. I, Reg. Papers*, vol. 52, no. 7, pp. 1276–1291, Jul. 2005.

[2] A. J. Lopez-Martin, J. Ramirez-Angulo, R. G. Carvajal, and L. Acosta, "Power-efficient class AB CMOS buffer," *Electron. Lett.*, vol. 45, pp. 89–90, Jan. 2009.

[3] J. Ramirez-Angulo, A. J. Lopez-Martin, R. G. Carvajal, and F. M. Chavero, "Very low-voltage analog signal processing based on quasi-floating gate transistors," *IEEE J. Solid-State Circuits*, vol. 39, no. 3, pp. 434–442, Mar. 2004.

[4] A. L. Martin, J. M. A. Miguel, L. Acosta, J. Ramirez-Angulo, and R. G. Carvajal, "Design of two-stage class AB CMOS buffers: A systematic approach," *Etri J.*, vol. 33, pp. 393–400, Jun. 2011.

[5] M. P. Garde, A. J. Lopez-Martin, and J. Ramirez-Angulo, "Power-efficient class-AB telescopic cascode opamp," *Electron. Lett.*, vol. 54, no. 10, pp. 620–622, 2018.

[6] A. Paul, J. Ramírez-Angulo, and A. Torralba, "Bandwidth-enhanced high current efficiency class-AB buffer with very low output resistance," *IEEE Trans. Circuits Syst. II, Exp. Briefs*, vol. 65, no. 11, pp. 1544–1548, Nov. 2018.

[7] S. Pourashraf, J. Ramirez-Angulo, A. J. Lopez-Martin, and R. González-Carvajal, "A highly efficient composite class-AB-AB miller op-amp with high gain and stable from 15 pF up to very large capacitive loads," *IEEE Trans. Very Large Scale Integr. (VLSI) Syst.*, vol. 26, no. 10, pp. 2061–2072, Oct. 2018.

[8] E. Cabrera-Bernal, S. Pennisi, A. D. Grasso, A. Torralba, and R. G. Carvajal, "0.7-V three-stage class-AB CMOS operational transconductance amplifier," *IEEE Trans. Circuits Syst. I, Reg. Papers*, vol. 63, no. 11, pp. 1807–1815, Nov. 2016.

[9] M. Jimenez, A. Torralba, R. G. Carvajal, and J. Ramirez-Angulo, "A new low-voltage CMOS unity-gain buffer," in *Proc. IEEE Int. Symp. Circuits Syst.*, May 2006, p. 4.

[10] J. Ramirez-Angulo, A. J. Lopez-Martin, R. G. Carvajal, A. Torralba, and M. Jimenez, "Simple class-AB voltage follower with slew rate and bandwidth enhancement and no extra static power or supply requirements," *Electron. Lett.*, vol. 42, pp. 784–785, Jul. 2006.

[11] K. Ogata, *Modern Control Engineering*, 5th ed. Upper Saddle River, NJ, USA: Prentice-Hall, 2010.

[12] B. Razavi, *Design of Analog CMOS Integrated Circuits* (Electrical and Computer Engineering). New York, NY, USA: McGraw-Hill, 2005.

[13] I. M. Filanovsky, J. Järvenhaara, and N. T. Tchamov, "Source follower: A misunderstood humble circuit," in *Proc. IEEE 56th Int. Midwest Symp. Circuits Syst. (MWSCAS)*, Aug. 2013, pp. 185–188.

$$Q = \frac{\sqrt{\left(1.2g''_{m1\text{P}} G_L + g_{m2P} g_{m1\text{P}}\right)[C_x(C_L + C_{\text{gs1P}}) + C_{\text{gs1P}} C_L (G_L/G_S)]}}{1.2g''_{m1\text{P}} C_x + G_L(C_L + C_{\text{gs1P}})} \quad \text{(2A)}$$

$$Z_{\text{Out}} = V_Y/I_Y = \frac{s^2(C_x C_{\text{gs1P}} R_S) + s(C_{\text{gs1P}} R_S G_L + C_X) + G_L}{s^2(C_{\text{gs1P}} C_X) + s(C_{\text{gs1P}} G_L + C_X g''_{m1\text{P}}) + (g_{m2P} g_{m1\text{P}}) + g''_{m1\text{P}} G_L} \quad \text{(3A)}$$

[14] J. T. Santos and R. G. Meyer, “A one-pin crystal oscillator for VLSI circuits,” *IEEE J. Solid-State Circuits*, vol. 19, no. 2, pp. 228–236, Apr. 1984.

[15] T. C. Carusone, D. Johns, and K. Martin, *Analog Integrated Circuit Design*, 2nd ed. Hoboken, NJ, USA: Wiley, 2012.

[16] J. Ramirez-Angulo, S. Gupta, R. G. Carvajal, and A. J. Lopez-Martin, “New improved CMOS class AB buffers based on differential flipped voltage followers,” in *Proc. IEEE Int. Symp. Circuits Syst.*, May 2006, pp. 3917-1–3917-4.

[17] C. Sawigun, A. Demosthenous, X. Liu, and W. A. Serdijn, “A compact rail-to-rail class-AB CMOS buffer with slew-rate enhancement,” *IEEE Trans. Circuits Syst. II, Exp. Briefs*, vol. 59, no. 8, pp. 486–490, Aug. 2012.

[18] G. Xing, S. H. Lewis, and T. R. Viswanathan, “Self-biased unity-gain buffers with low gain error,” *IEEE Trans. Circuits Syst. II, Exp. Briefs*, vol. 56, no. 1, pp. 36–40, Jan. 2009.

[19] A. J. Lopez-Martin, E. Osés, J. Ramírez-Angulo, and R. G. Carvajal, “Micropower class AB voltage followers with simple quiescent current control,” in *Proc. IEEE 55th Int. Midwest Symp. Circuits Syst. (MWSCAS)*, Aug. 2012, pp. 218–221.

Anindita Paul (M’16) was born in Chinsurah, India. She received the M.Tech. degree in VLSI design from the Institute of Radio Physics and Electronics, University of Calcutta, Kolkata, India. She is currently working toward the Ph.D. degree at the Klipsch School of Electrical Engineering, New Mexico State University, Las Cruces, NM, USA.

Her current research interests include low-voltage low-power analog circuit design.

Jaime Ramírez-Angulo (M’82–F’00) received the B.Sc. degree in communications and electronic engineering (Professional degree) and the M.S.E.E. degree from the National Polytechnic Institute, Mexico City, Mexico, in 1974 and 1976, respectively, and the Ph.D. degree from the University of Stuttgart, Stuttgart, Germany, in 1982.

He was a Professor with Texas A&M University, College Station, TX, USA. He is currently a Distinguished Award Professor with the Klipsch School of Electrical and Computer Engineering, New Mexico State University, Las Cruces, NM, USA, where he is also the Director of the Mixed-Signal VLSI Laboratory. He is also with the National Institute of Astrophysics, Optics and Electronics (INAOE), Cholula, Mexico. His current research interests include various aspects of design and test of analog and mixed-signal very large-scale integrated circuits.

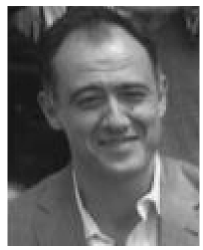

Antonio Torralba (M’89–SM’02) received the M.Sc. degree in industrial engineering with a minor in electrical engineering and the Ph.D. degree from the University of Seville, Seville, Spain, in 1983 and 1985, respectively.

Since 1983, he has been with the Department of Electronics Engineering, School of Engineering, University of Seville, where he was an Assistant Professor, an Associate Professor from 1987 to 1996, and the Director of the Department from 2008 to 2016. He has also been a Professor with the University of Seville since 1996, where he currently leads a research group on mixed signal design. He was a Visiting Researcher with the Klipsch School of Electrical Engineering, New Mexico State University, Las Cruces, NM, USA, in 1999, and with the Department of Electrical Engineering, Texas A&M University, College Station, TX, USA, in 2004. He has coauthored 90 papers in international journals. His research interests include low-power low-voltage analog and mixed signal microelectronics.